Chemical Engineering Journal 163 (2010) 78–85

Contents lists available at ScienceDirect

Chemical Engineering Journal

journal homepage: www.elsevier.com/locate/cej

Deep-bed filtration model with multistage deposition kinetics

Vitaly Gitis [a,*], Isaak Rubinstein [b], Maya Livshits [c], Gennady Ziskind [c]

[a] Unit of Environmental Engineering, Ben-Gurion University of the Negev, P.O. Box 653, Beer-Sheva 84105, Israel
[b] Blaustein Institutes for Desert Research, Ben-Gurion University of the Negev, Sede Boqer Campus 84990, Israel
[c] Department of Mechanical Engineering, Ben-Gurion University of the Negev, P.O. Box 653, Beer-Sheva 84105, Israel

ARTICLE INFO

Article history:
Received 1 June 2010
Received in revised form 11 July 2010
Accepted 19 July 2010

Keywords:
Deep-bed filtration
Porous media
Mathematical modeling
Accumulation kinetics
Particle
Packed bed

ABSTRACT

In the present study, a phenomenological model of deep-bed filtration is suggested. It combines an advection-dispersion equation with an equation of nonlinear multistage accumulation kinetics. The model includes dispersion and accounts for temporal and spatial changes in media porosity.

It is suggested that at any location inside the column the filter deposit is formed first as an irreversible ripening layer, followed by formation of reversible deposit during the operable stage. The latter continues until the deposit reaches locally its maximum value. Then, filter breakthrough takes place.

The equations are solved numerically, using an explicit finite-difference scheme. The results compare favorably with laboratory experiments at an EPA facility, and with field experiments performed by Mekorot–Israeli Water Company.

1. Introduction

Rapid granular filtration is one of the widely implemented treatment methods for relatively dilute aqueous suspensions. In this method, the grains of a porous medium, like sand, anthracite, tuff, etc., adsorb up to 85% by mass of suspended particles [1], transported by water inside the filter bed. To ensure a high quality of the tap water, it is essential to understand filtration kinetics and to predict filter performance through physically sound modeling.

The beginning of deep-bed filtration theory dates back to more than a half-century ago and is associated with the works of Iwasaki [2] and Minz [3]. Filtration models are commonly classified as phenomenological, stochastic or trajectory ones [4]. In spite of the fact that the latter are better justified, their practical application is limited to simple geometric representations that reflect clean bed conditions only. Experimental validation of the trajectory models often has limited success, thus requiring introduction of numerous empirical coefficients, typical of stochastic and phenomenological models, whereas the latter ones often incorporate implicitly some information about the stochastic aspects of mass transfer.

The deep-bed filtration can basically be viewed on a macroscopic or microscopic level. The microscopic view is usually presented as a sequence of transport and attachment steps where the transport is discussed in view of five transport mechanisms, namely interception, inertia, diffusion, sedimentation and local turbulence [5] and the attachment is viewed through the van der Waals attraction and electrostatic repulsion of two entities, a particle and a media grain. This allows obtaining a "filter coefficient" which is then introduced into a macroscopic model. State-of-the art of the macroscopic filtration modeling of hydrosols and aerosols is presented in a recent book by Tien and Ramarao [6]. Apparently, such models are widely used also in petroleum engineering. For instance, Guedes et al. [7] analyze deep-bed filtration under multiple particle-capture mechanisms and conclude that it is possible to reflect them in a single coefficient. A review paper by Zamani and Maini [8] analyzes microscopic and macroscopic models, discussing advantages of the latter in prediction of the removal efficiency of deep-bed filtration process. It is stated that predicting the filter performance by a macroscopic model requires the knowledge of filter coefficient, which can be obtained by using a search optimization technique along with effluent concentration history. Alvarez et al. [9] argue that the filtration function, which is the fraction of particles captured per unit particle path length, cannot be measured directly and thus must be calculated indirectly by solving inverse problems. As the practical petroleum and environmental engineering situations require knowledge of particle penetration depth, they determine this quantity from effluent concentration histories measured in one-dimensional laboratory experiments.

Macroscopically, filtration process may be described as a change in concentration, C, of the suspended particles with time, t, whereas a local mass conservation law is combined with an accumulation kinetics' equation. The kinetic equation for particle capturing process is generally expressed as $\partial\sigma/\partial t = F(C, \sigma)$, where σ is the specific deposit, defined as the amount of material deposited per

* Corresponding author.
E-mail address: gitis@bgu.ac.il (V. Gitis).

1385-8947/$ – see front matter © 2010 Elsevier B.V. All rights reserved.
doi:10.1016/j.cej.2010.07.044

Nomenclature

a_L	coefficient of longitudinal dispersivity, m
C	mass concentration of particles in suspension, kg/m^3
d_c	average diameter of filter grain, m
d_p	average particle diameter, m
D	effective dispersion coefficient, m^2/h
j	particle flux, kg/m^2 h
K_a	attachment rate coefficient in the operable stage, 1/m
K_d	detachment rate coefficient in the operable stage, 1/h
K_r	attachment rate coefficient in the ripening stage, 1/m
L	filter depth, m
t	time, h
u	longitudinal approach velocity, m/h
z	position in the column measured as a distance in longitudinal direction (direction of flow), m

Greek letters

Λ	diffusion number in numerical scheme
γ	Courant number in numerical scheme
ε	local bed porosity at time t
λ	filter coefficient, 1/m
μ	absolute viscosity of suspension, kg/m h
ρ	density of particle material, kg/m^3
σ	specific deposit, kg/m^3
σ_r	transient specific deposit, kg/m^3
σ_u	ultimate specific deposit, kg/m^3

Operator

$\tilde{B}$	dimensionless form of variable B

Subscript

0	initial value

unit volume of the filter. An analysis of the existing literature shows [6,10] that there exist two alternative approaches to $F(C,\sigma)$, which reflect the accumulation kinetics:

(1) Irreversible accumulation, meaning that a suspended particle, once retained by the porous bed, is never entrained by the flow again [2,11–14]. The respective equations of attachment kinetics of this type have the general form of $\partial\sigma/\partial t = \lambda Cu$, with various models differing in the way of specifying the filter coefficient, λ. Generally, λ is not constant throughout the filtration process.
(2) Reversible accumulation, meaning that a suspended particle is alternately deposited and ripped off by the flow [3,15]. The respective equation of accumulation kinetics is $\partial\sigma/\partial t = K_a uC - K_d\sigma$, with the phenomenological attachment and detachment coefficients, K_a and K_d, specified empirically.

The main difference between the two approaches lies in their treatment of an experimentally evidenced breakthrough stage of filtration, where the presence of suspended particles increases [16]. According to the first approach, the breakthrough occurs when the media pores become so narrow that under constant feed the interstitial velocity does not allow the suspended particles to adhere [11,17]. The second approach implies that tearing of discrete (original) particles off the deposit by shear forces is as obvious as in flocculation [18].

The models reported in the literature have greatly enhanced our understanding of the mechanisms behind deep-bed filtration and provided useful insights in specific practical applications. An analysis of the literature shows, however, that the existing models are mutually excluding: they imply that the filtration cycle contains either the ripening and operation stages, as in an irreversible deposition mode, or operation and breakthrough stages, as in a reversible deposition mode. Thus, each of these two approaches disregards one of the stages of the filtration process evidenced from the experiments [16]. Being aware of this problem, the followers of the irreversible approach introduced complex filtration coefficients [5] that at a certain level of the specific deposit caused decrease in filtration efficiency, in order to account for the breakthrough stage. On the other hand, in the reversible deposition models a dashed line is commonly hand-added to the predicted filtration curves in order to reflect the excluded ripening stage [15]. Thus, in any of the approaches the full filtration cycle was not predicted or at least reflected. As a result, an accurate representation of the entire cycle was difficult if not impossible [19].

The model suggested herein fuses the kinetic approaches previously viewed as mutually excluding. It comprises two differential equations: a full mass balance equation and a multistage-kinetics equation. Specifically, at any given depth inside the filter, the model differentiates between the following three stages in the accumulation of suspended particles:

(1) Ripening stage – irreversible formation of deposit monolayer on filter medium.
(2) Operable stage – consequent reversible deposit growth.
(3) Breakthrough stage – halt of further accumulation upon reaching, locally, a certain amount of the deposited material.

A closed system of coupled partial and ordinary differential equations, with appropriate boundary and initial conditions, is solved numerically by the method of finite differences. The results of the full numerical solution are analyzed and compared with the performance of a laboratory-scale filtration plant which was designed and constructed specifically for this task. In addition, the model predictions are compared with the data of field experiments performed by the Mekorot Water Company in Israel.

2. Model

The model suggested herein is based on the following physical picture. An aqueous dilute colloidal suspension is fed through a filter bed which initially contains no deposit. At the beginning, passing colloids may settle as separate particles covering filter grains with a monolayer deposit [14]. This is the ripening stage recognized in filtration concentration plots by relatively low retention. The ripening lasts until the upstream surface of media grains becomes coated with single particles, or until the occasional dendrites formed on the grains evolve into a monolayer through proliferation onto the uncovered part of the grain surface [13,20]. Once the born particles start to interact primarily with the previously deposited ones, the retention efficiency increases and the filtration cycle is entering the operable stage. Here, both attachment of the suspended particles and their re-entrainment by the flow occur in parallel [21]. The transition from the irreversible to reversible deposition mode takes place when the specific deposit attains a prescribed transitional value, σ_r.

Since the volume of particles that can be hold by the filter is finite, eventually a saturation stage is achieved when the bed local specific deposit reaches its maximum feasible value, σ_u. From this moment on, it is assumed that further accumulation effectively

stops at that location, and thus any suspended particles are only transferred along the transport channels formed in the bed [22,23].

The approach adopted in the present study is based on the assumption that particle concentration in the stream, C, is uniform across the filter cross-section. Also, the approach velocity, u, is assumed to be uniform. Accordingly, the expected specific deposit, σ, is uniform across the cross-section, too. These common assumptions mean that the present model is one-dimensional in space, i.e. both the concentration and specific deposit depend on the z-coordinate, which denotes the filter depth, and also on time.

Each filter bed slice between the cross-sections at z and $z+\Delta z$ is characterized by mass balance comprised by the following four factors: incoming particle flux j_z, outcoming particle flux $j_{z+\Delta z}$, rate of particle deposition/re-entrainment $\partial\sigma/\partial t$, and the resulting rate of change of particle concentration in the feed, $\partial C/\partial t$. Accordingly, the species conservation equation attains the following form:

$$\frac{\partial \varepsilon C}{\partial t} + \frac{\partial \sigma}{\partial t} = -\frac{\partial}{\partial z} j \tag{1}$$

It is important to note that the first term on the left-hand side of Eq. (1) includes also the local porosity, ε, and this in order to take into account the changes in the fluid volume due to the increasing deposit. It is obvious that ε is time-dependent at any location inside the bed.

The particle flux, j, includes both dispersion and convection contributions:

$$j = uC - \varepsilon D \frac{\partial C}{\partial z} \tag{2}$$

where D is the effective dispersion coefficient.

The outlined above three different stages of filtration are described by the following kinetic equation for the accumulation rate, $\partial\sigma/\partial t$:

$$\frac{\partial \sigma^{\mathrm{def}}}{\partial t} = \begin{cases} K_r uC & \text{when} \quad 0 < \sigma \le \sigma_r \\ K_a uC - K_d \sigma & \text{when} \quad \sigma_r < \sigma < \sigma_u \\ 0 & \text{when} \quad \sigma = \sigma_u \end{cases} \tag{3}$$

where K_r is the attachment rate coefficient at the ripening stage; K_a is the attachment rate coefficient at the operable stage; K_d is the detachment rate coefficient at the operable stage; σ_r is a threshold specific deposit value, corresponding to the transition from the ripening to the operable stage; and σ_u is the ultimate specific deposit value, which indicates the filter retention capacity limit. It is important to emphasize that the values of σ are compared to the preset limits, σ_r and σ_u, locally, reflecting the real situation in which various stages coexist inside the filter bed at the same instant, depending on the cross-section location. It is worth to note also that the expression of Eq. (3) defines the general case of multistage transition and might be reduced to particular cases of irreversible and reversible attachment [15,24].

The local porosity, ε, is related to its initial value ε_0 and the specific deposit σ through the relation

$$\varepsilon = \varepsilon_0 - \frac{\sigma}{\rho} \tag{4}$$

where ρ is the physical deposit layer density, assumed constant for simplicity.

Eqs. (1–4) form a closed system of coupled partial and ordinary differential equations for $C(z,t)$ and $\sigma(z,t)$, which requires a set of appropriate boundary and initial conditions. Reflecting a constant or near constant concentration of impurities in the feed water taken from a large reservoir, a specific, constant concentration of particles in the feed suspension is assumed at the entrance to the column:

$$C = C_0 \quad \text{at} \quad z = 0, \quad t > 0 \tag{5}$$

The Danckwerts exit criterion [25], which assumes that there is no concentration change at the exit from the filter bed, is adopted as the second boundary condition:

$$\frac{\partial C}{\partial z} = 0 \quad \text{at} \quad z = L, \quad t > 0 \tag{6}$$

The initial conditions correspond to a clean bed before the filtration starts:

$$C(z, 0) = 0 \tag{7}$$

$$\sigma(z, 0) = 0 \tag{8}$$

The complete model presented above requires a numerical solution, which will be discussed in the next section. We note that upon setting $D = 0$, $\varepsilon = \text{const}$, $\sigma_r \to \infty$, the system of Eqs. (1–4) is reduced to the much simpler case of a linear attachment-advection model. The latter yields a classical Cauchy problem for a first-order linear hyperbolic equation, and may be solved in a straightforward manner by the method of characteristics [26]. However, such solution would be practically limited to the first filtration stage.

3. Numerical solution

The initial/boundary value problem, defined by Eqs. (1–8), is solved numerically by the method of finite differences. For this purpose, the equations are rendered dimensionless, using the following definitions:

$$\tilde{z} = \frac{z}{L} \quad \tilde{t} = \frac{ut}{L} \quad \tilde{\sigma} = \frac{\sigma}{C_0} \quad \tilde{C} = \frac{C}{C_0} \tag{9}$$

where L is the filter length, u is the approach velocity, and C_0 is the concentration at the entrance to the filter.

An explicit algorithm is used for the numerical solution. From the stability considerations, a backward–forward finite-difference scheme has been chosen, with the first-order backward advective derivative and forward time derivative. The dispersion term was approximated using a second-order central difference scheme. The specific deposit σ was calculated by a fourth-order Runge–Kutta scheme [27]. The filter length was subdivided into 100 equal grid steps.

To ensure stability of the implemented scheme, the time step is limited by the criteria based on the Courant number, γ, and diffusion number, Λ, respectively defined as:

$$\gamma = \frac{\Delta \tilde{t}}{\Delta \tilde{z}}$$

$$\Lambda = \frac{1}{Pe} \frac{\Delta \tilde{t}}{\Delta \tilde{z}^2} \tag{10}$$

where $\Delta\tilde{t}$ and $\Delta\tilde{z}$ are the dimensionless time and space steps, respectively, and the "numerical" mass Peclet number is defined as $Pe = u\Delta z/D$, according to [28,29]. It has been found empirically that in order to ensure stability, the values of γ and Λ must be smaller than 0.4, which is slightly more conservative than $\gamma < 1$ and $\Lambda < 0.5$ found in the literature [29].

Data input for each numerical simulation includes the filter depth, approach velocity and approximate run time. The computer code is written in Visual C++.

As shown in the previous section, formulation of the problem requires determination of a number of quantities, including the hydrodynamic dispersion coefficient, D, attachment rate coefficients in the ripening and operable stages, K_r and K_a, respectively, detachment rate coefficient in the operable stage, K_d, threshold specific deposit, σ_r, and ultimate specific deposit, σ_u. The values of these parameters are assigned based on the literature, even though

Table 1
Parameter values used in the test runs.

Parameter		Units	The range	The references
Initial porosity	ε	–	0.4	0.41 [38] 0.39 [39] 0.35 [40]
Attachment rate coefficient in the ripening stage	K_r	1/m	0.8–2.5	3.1 [32] 1.5 [33]
Attachment rate coefficient in the operable stage	K_a	1/m	6–9	10–12 [41] 5–12 [42] 12–15 [15] 3–150 [40] 10–90 [43] 20–30 [44]
Detachment rate coefficient in the operable stage	K_d	1/h	2×10^{-4}–2×10^{-3}	1.5×10^{-4}–2×10^{-4} [42] 1.5×10^{-3} [45] 1.3×10^{-6} [15] 2.2×10^{-5}–1.6×10^{-3} [40]
Transient specific deposit	σ_r	mg/cm^3	0.1–0.35	
Ultimate specific deposit	σ_u	mg/cm^3	9.5–20	130 [14] 42–60 [39] 20–70 [15]

their accuracy may be questionable [5]. The values found in the literature are summarized in Table 1. One can see that each parameter is represented by a range rather than by a specific value.

The hydrodynamic dispersion coefficient, D, can be estimated as

$$D \sim a_L u \tag{11}$$

where a_L is the coefficient of longitudinal dispersivity. It was found experimentally that it is of the order of magnitude of the average sand grain size [30]. For instance, for the grain diameter of 1 mm, we have $a_L \sim 10^{-3}$ m, which for the typical approach velocities of several dozens of meters per hour yields $D \sim 10^{-6}$–10^{-5} m^2/s.

In the suggested model, ripening is a fast irreversible process characterized by interactions between particles and media grains. Accordingly, the attachment rate coefficient, K_r, may be assumed constant throughout this stage. This is different from the previous models [11,13,31], where the particle–particle collisions are assumed to determine the entire run, thus prescribing changes in the filtration coefficient even during the ripening stage. The assumption of constant K_r allows its computation based on the initial filter coefficient for a clean bed, λ_0. For this purpose, the trajectory models of Choo and Tien [32] and Rajagopalan and Tien [33] were used. For the conditions defined in the caption of Fig. 1, the values of K_r = 3.1 and 1.5 m^{-1} were obtained. Based on these results and on a comparison with experimental data, the values in a range of 0.8–2.5 m^{-1} were used for K_r in our calculations, as presented in Table 1.

The attachment rate coefficient at the reversible growth stage, K_a, is higher than K_r. This result, evident from a general form of the concentration plot and generally agreed among the researchers, is caused by a transition from particle–bed interactions at the ripening stage to particle–particle interactions at the operable stage. Whereas the previous models were based on a continuous improvement of the filter coefficient as a function of the specific deposit, we assume that there is no significant change in the attachment rate coefficient within a certain stage. Therefore, the attachment rate coefficient at the reversible growth stage, K_a, is considered constant. Table 1 summarizes its values reported in the literature. One can see that considerable deviations exist between the results reported by different researchers.

Although some expressions for the detachment rate coefficient, K_d, are suggested in the literature [34], its experimentally found values fluctuate significantly between various filtration sites as a result of the differences in suspension composition, filter material, filtration regime, and a variety of other factors. In the current study, the values of K_d were estimated by averaging its values reported in the literature for the models with reversible deposition kinetics [3,15], see Table 1.

It is quite difficult to evaluate the specific deposit threshold value, σ_r, in the absence of direct experimental data. Based on physical considerations, its order of magnitude can be estimated for given conditions assuming that it corresponds to the most dense particle monolayer on the upper half of grain surface. For instance, for the grain diameter of 1 mm and particle diameter of 1 μm, the value of σ_r would not exceed 0.5 mg/cm^3, i.e. the order of unity when expressed in milligrams per cubic centimeter.

Whereas the operable stage is characterized by an increase in the effective hydraulic diameter of the grain due to the attached deposit, the subsequent breakthrough stage involves formation of transport channels inside the filter bed. This transition occurs locally when the specific deposit reaches the threshold value, σ_u, which depends on media grain, filtration velocity, coagulation/flocculation regime and several other factors. The only model that considered the deposition mode transition was suggested by Tien et al. [14], who indicated that the pores were blocked at 50 mg/cm^3. It was suggested to determine the value of σ_u based

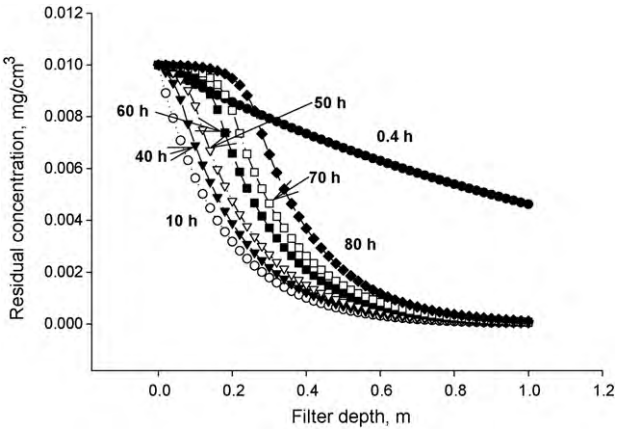

Fig. 1. Calculated distribution of residual concentration in filter depth for time periods of 0.4, 10, 40, 50, 60, 70, 80 h. Parameter values: u = 10 m/h; L = 1 m; C_0 = 10 mg/L = 0.01 mg/cm^3; $D = 2.8\times10^{-4}$ m^2/s; d_p = 10 μm = 10^{-5} m; d_g = 1 mm = 10^{-3} m; $\mu = 10^{-3}$ kg/m/s (20 °C); ρ_w = 998.2 kg/m^3 (20 °C); ρ_p = 1500 kg/m^3; ε_0 = 0.4; K_r = 0.8 1/m; K_a = 7.5 1/m; $K_d = 2\times10^{-4}$ 1/m; σ_r = 0.2 kg/m^3; σ_u = 20.0 kg/m^3 = 20.0 mg/cm^3.

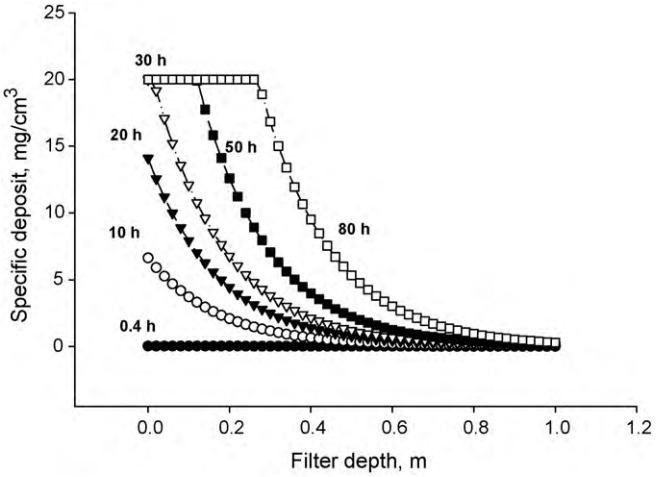

Fig. 2. Calculated distribution of specific deposit in filter depth for time periods of 0.4, 10, 20, 30, 50, 80 h. Parameter values are similar to those detailed for Fig. 1.

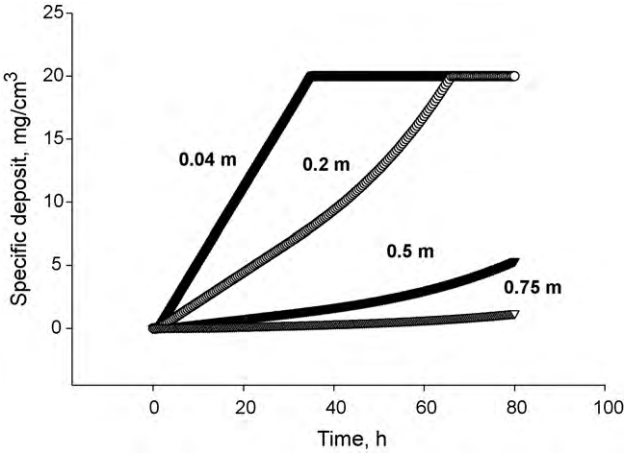

Fig. 4. Calculated specific deposit as a function of run time for depths of 0.04, 0.2, 0.5, 0.75 m. Parameter values are similar to those detailed for Fig. 1.

on the best-fit method. The experimentally found values were in the range of 9.5–20 mg/cm^3.

4. Test runs of the model

The presented above model was run to obtain the results shown in Figs. 1–5. A hypothetical 1-m-deep column, fed with a dilute solution at the approach velocity of 10 m/h, was simulated using the parameters listed in Table 1. Simulations included effects on particle removal and specific deposit accumulation of such parameters as the run time, suspended particles' concentration, bed depth, deposit layer density, initial bed porosity, attachment rate coefficients in the ripening and operable stages, K_r and K_a, respectively, detachment rate coefficient in the operable stage, K_d, transient specific deposit, σ_r, and ultimate specific deposit, σ_u. Some essential findings are presented in Figs. 1–5. It is worth to note that the curves in these figures reflect the well-known filter operation curve observed in experiments and reported in the literature. Recall that the full curve generally has three stages: ripening, efficient filtration and breakthrough [16]. The calculated curves, presented in Figs. 1–5, are intentionally focused on specific stages of filtration, and thus not necessarily represent the entire cycle. This is done in order to allow a discussion of subtle details.

Fig. 1 shows the local concentration as a function of the depth for various instants ranged from 24 min (0.4 h) to 80 h. The observed curves can be subdivided into three cases: an almost linear decrease from the entrance to the column, observed at 0.4 h; an exponential decrease from the entrance to the column, observed at 10, 40, 50 and 60 h; and an exponential decrease which starts somewhere inside the column, observed at 70 and 80 h. Here, the linear decrease at 0.4 h corresponds to the first, irreversible, filtration stage that is characterized by minor changes in the deposit along the filter. The curves at 10, 40, 50 and 60 h correspond to the second, operable, filtration stage for the entire filter. Here, the specific deposit value exceeds σ_r = 0.2 mg/cm^3 but does not reach σ_u = 20 mg/cm^3. Finally, the curves for 70 and 80 h correspond to a situation in which a significant amount of the sediment had been accumulated in the filter. As a result, no changes in the residual concentration are observed in the filter part located close to the entrance. In Fig. 1, the depths of 0.2 and 0.3 m, for 70 and 80 h respectively, have only a minor effect on the residual concentration. This observation corresponds to the specific deposit saturation, σ_u, achieved at a given depth, meaning that the corresponding part of the filter only transfers the particles while their concentration is not affected.

The corresponding changes in the specific deposit, σ, as a function of bed depth for various instants, are depicted in Fig. 2. The presented data allow direct tracking of the three-stage deposition kinetics. For example, the plot shows that the specific deposit at 0.4 h is lower than σ_r = 0.2 mg/cm^3 and, accordingly, the deposition evolves slowly. At 10, 20, and 30 h of filtration, the rate of depo-

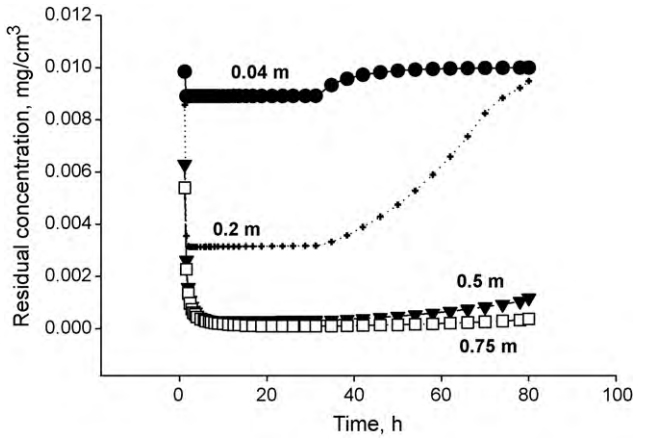

Fig. 3. Calculated residual concentration as a function of run time for depths of 0.04, 0.2, 0.5, 0.75 m. Parameter values are similar to those detailed for Fig. 1.

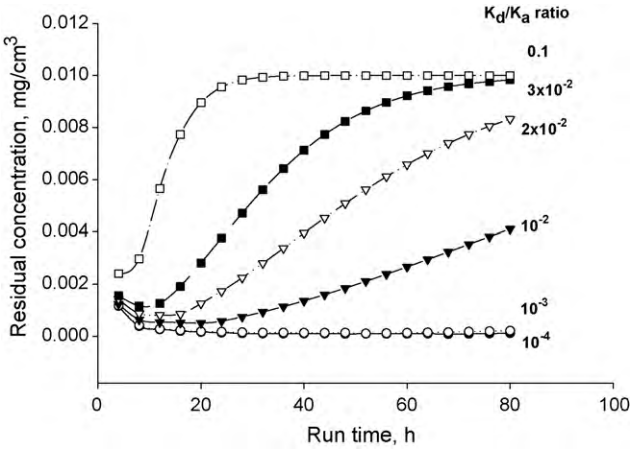

Fig. 5. Calculated residual concentration as a function of run time for various K_d/K_a ratios. Parameter values are similar to those detailed for Fig. 1 except for K_d values of 0.75, 0.25, 0.15, 0.075, 0.0075, 0.00075 1/m.

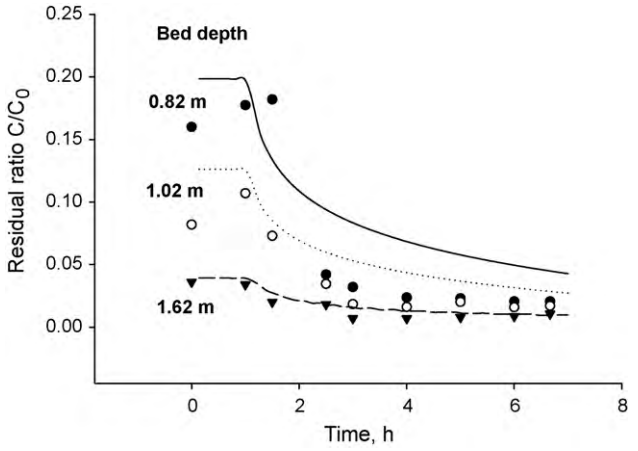

Fig. 6. Experimental data (dots) and model prediction (curves) for the experiments performed at US EPA T&E Facility for bed depths of 0.82, 1.02 and 1.62 m. Parameter values: $u = 10$ m/h; $L = 1.62$ m; $K_r = 2.5$ 1/m; $K_a = 9$ 1/m; $K_d = 5 \times 10^{-3}$ 1/h; $\sigma_r = 0.35$ mg/cm^3; $\sigma_u = 20.0$ mg/cm^3.

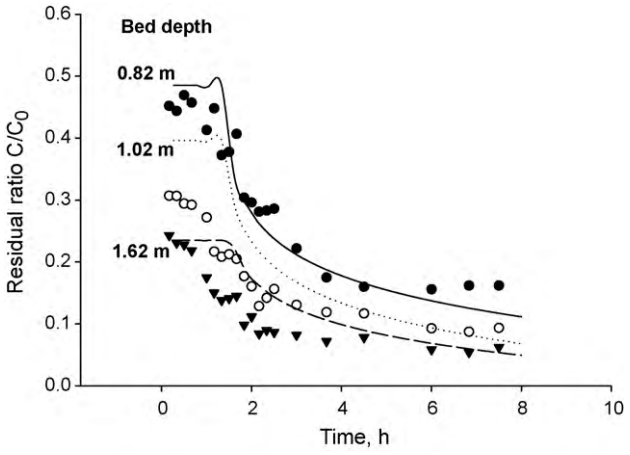

Fig. 7. Experimental data (dots) and model prediction (curves) for the experiments performed at US EPA T&E Facility for bed depths of 0.82, 1.02 and 1.62 m. Parameter values: $u = 10$ m/h; $L = 1.62$ m; $K_r = 1.2$ 1/m; $K_a = 7.5$ 1/m; $K_d = 5 \times 10^{-3}$ 1/h; $\sigma_r = 0.2$ mg/cm^3; $\sigma_u = 20.0$ mg/cm^3.

sition increases yet the entire filter is in the operable stage. After 30 h, the retention capacity of the top 5 cm layer exceeds the set σ_u level of 20 mg/cm^3. Referring to Fig. 1, this means that the residual concentration in the upper 5 cm of the filter does not change. The deeper lying layers of the column are taken out of action one after the other. As a result, the retaining effect of the column deteriorates. This is reflected in a gradual increase in the residual concentration at a given location within the column, which lasts until the concentration at that location is the same as at the entrance, meaning that the entire part of the column between the entrance and the location concerned is saturated.

Fig. 3 shows the concentration vs. time, while the depth serves as the parameter. One can see that for any given depth, the concentration first decreases steeply, then remains practically constant, and finally increases back to its maximum value. Actually, the first stage precedes the steep decrease, which indicates that the transition to reversible accumulation has begun. The curves for different depths are similar, but it is obvious that deeper into the column lower concentrations are reached, and this is because of filtration by a thicker bed. For any depth, the concentration eventually attains the same value as at the entrance, but this happens much later for deeper locations. As follows from Fig. 4, the deposit at any given depth also reaches its maximum value eventually, first close to the entrance and then throughout the filter towards the exit.

Fig. 5 shows an effect of the detachment-attachment ratio, K_d/K_a, on the concentration at the exit. It is obvious that the lower this ratio, the lower the concentration achieved, and the longer the time for which the concentration remains at its minimum. Thus, Figs. 1–5 indicate that the model yields physically meaningful predictions of well-established filtration stages [16].

5. Comparison with experiments

Two types of comparisons are presented in Figs. 6–9, and this in order to demonstrate the ability of the model to predict the filtration results under a broad variety of experimental conditions. Figs. 6 and 7 present the laboratory experiments, whereas the results of Figs. 8 and 9 have been obtained in field experiments performed by the Mekorot Water Company at Eshkol site [35].

The experiments reflected in Figs. 6 and 7 have been performed by Gitis [36,37] at U.S. EPA Test and Evaluation (T&E) Facility in Cincinnati, Ohio. A special pilot-scale filtration system was designed and built. A 2.6 m high, 0.17 m in diameter acrylic transparent filter column had 9 sampling and 9 pressure ports,

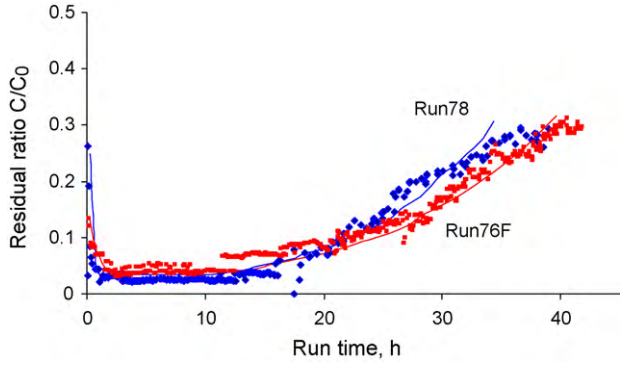

Fig. 8. Experimental data (dots) and model prediction (curves) for the experiments performed by Mekorot. Parameter values: $u = 25$ m/h; $L = 1.7$ m; $K_r = 0.5$–0.7 1/m; $K_a = 8.5$–9 1/m; $K_d = 2 \times 10^{-3}$ 1/h; $\sigma_r = 0.1$ mg/cm^3; $\sigma_u = 9.5$–10.2 mg/cm^3.

located in pairs from opposite sides of the column. Sampling points were inserted 0.05 m inside the column to avoid wall effect that misinterprets filtrate quality. The column was packed with 1.6 m of uniform size sand having geometric mean diameter of 1.05 mm and uniformity coefficient of 1.55. The media porosity, determined by volumetric measurements, was 0.44. The size and characteristics of the set-up were chosen in order to reflect practical filtration conditions. In particular, the filter had to be deep enough to allow the overall filtration parameters to be valid. On the other hand,

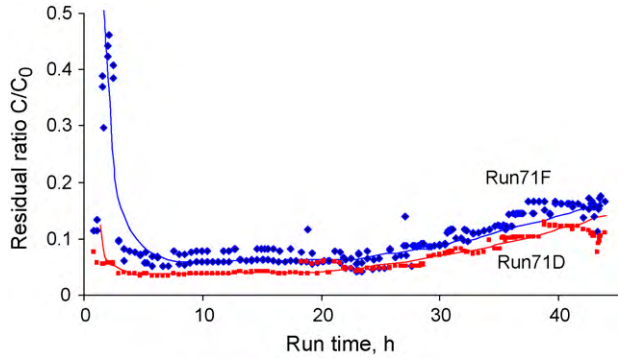

Fig. 9. Experimental data (dots) and model prediction (curves) for the experiments performed by Mekorot. Parameter values: $u = 20$ m/h; $L = 1.7$ m; $K_r = 0.6$–1.2 1/m; $K_a = 6$–7 1/m; $K_d = 2 \times 10^{-3}$ 1/h; $\sigma_r = 0.1$–0.2 mg/cm^3; $\sigma_u = 12$–12.5 mg/cm^3.

the above mentioned 9 sampling and 9 pressure ports allowed to monitor smaller depths during the same runs.

A slurry, which consisted of Kaolin clay particles and Cincinnati tap water, was pumped into a 1000 L cross-linked polyethylene (XLPE)-made feed tank. Suspension in the tank was kept completely mixed by using a high-speed mixer. A centrifugal pump was used to lift the suspension into a 100 L head tank located 3.6 m above the filtration column. Water level in the feed tank was maintained at a constant height by an overflow line returning the suspension to the feed tank. The column was operated at a constant flow rate of 5 and 10 m/h, under the contact (in-line) filtration mode in the conventional downward direction. The filtration velocity was controlled and adjusted by a flowmeter connected to the column outlet. Immediately after each run, filter was backwashed for 1 min by airflow at 200 kN/m^2, and then for 10 min by a reversed flow of Cincinnati tap water at 1.1 L/s.

Figs. 6 and 7 show the residual concentration evolution at three different bed depths: 0.82, 1.02 and 1.62 m, for two different experimental runs. A typical numerical run takes about an hour and a half on a PC, which may be considered as relatively fast. One can see that a reasonable agreement is achieved between the model predictions and the experiments, with the following values of model parameters: $K_r = 2.5$ and 1.2 1/m, $K_a = 9$ and 7.5 1/m, $\sigma_r = 0.35$ and 0.2 mg/cm^3 for Figs. 6 and 7, respectively, $K_d = 0.005$ 1/h, $u = 10$ m/h, and $\sigma_u = 20$ mg/cm^3. In particular, the first two stages of filtration, irreversible and operable, are clearly observed. It can be seen that, although an explicit scheme is used, no oscillating or non-monotonic profiles are encountered. We note that the runs were not sufficiently long to achieve the third, breakthrough, stage.

In Fig. 8, the model is compared to two different field experiments. The filtration velocity is 25 m/h. One can see that a good agreement between the predictions and the experimental results is achieved for the entire filtration process with the following parameters: $u = 25$ m/h, $L = 1.7$ m, $K_r = 0.5$–0.7 1/m, $K_a = 8.5$–9 1/m, $K_d = 2 \times 10^{-3}$ 1/h, $\sigma_r = 0.1$ mg/cm^3, $\sigma_u = 9.5$–10.2 mg/cm^3. In particular, it appears that the model predicts the late stage of the process rather accurately.

In Fig. 9, the model is compared to the field experiments represented by two different runs in the same filtration column. Again, a good agreement is observed. It is worth to note that the values of the parameters used in the simulations are the same as in Fig. 8, except for K_a and σ_u, which also are rather close (9 vs. 7 and 10.2 vs. 12.5, respectively). These differences, which probably reflect variations that exist in the industrial system used in the experiments, do not contradict to the general applicability of the model presented herein.

6. Conclusions

In the present study, a phenomenological model of deep-bed filtration is suggested. It combines an advection-dispersion equation with an equation of nonlinear multistage accumulation kinetics. It is assumed that at any location inside the column, the filter deposit is formed first as an irreversible ripening layer, followed by the formation of a reversible deposit during the operable stage. The latter continues until the deposit reaches locally its maximum value. Then, filter breakthrough takes place. Thus, the suggested model is able to represent the entire filtration cycle. The model also includes dispersion and accounts for temporal and spatial changes in media porosity.

The equations have been solved numerically, using an explicit finite-difference scheme. The parameter values were set in the ranges reported in the literature. Time and space dependence of the residual concentration and specific deposit are revealed. Furthermore, predictions of the model are compared with the available experimental data. The results are in a good agreement with both laboratory experiments at a U.S. EPA facility and field experiments performed by Mekorot–Israeli Water Company.

The calculations suggest that the major parameters of the model, which determine the general shape of the filtration curves, are the attachment rate constant, K_a, and the lower and upper deposit thresholds of the reversible accumulation stage, σ_r and σ_u, respectively. At the same time, the other two parameters of the kinetic model, namely the primary accumulation rate, K_r, and the detachment rate, K_d, have relatively minor effects at standard filtration conditions.

Acknowledgements

This research was supported by the Israel Science Foundation (grant no. 1184/06). We thank Dr. Samir Hatukai for pilot filtration data.

References

[1] J.L. Cleasby, G.S. Logsdon, Granular bed and precoat filtration, in: R.D. Letterman (Ed.), Water Quality and Treatment: A Handbook of Community Water Supplies, AWWA, 5th ed., McGraw-Hill, New York, 1999.
[2] T. Iwasaki, Some notes on sand filtration, Journal of American Water Works Association 29 (5) (1937) 1591–1602.
[3] D.M. Minz, Kinetics of filtration of low-concentration water suspensions in water purification filters, Doklady Akademii Nauk SSSR 78 (1951) 315–318 (in Russian).
[4] A. Amirtharajah, Some theoretical and conceptual views of filtration, Journal American Water Works Association 80 (1988) 36–46.
[5] K.J. Ives, Rapid filtration, Water Research 4 (1970) 201–223.
[6] C. Tien, B.V. Ramarao, Granular Filtration of Aerosols and Hydrosols, 2nd ed., Elsevier, 2007.
[7] R.G. Guedes, F. Al-Abduwani, P. Bedrikovetsky, P.K. Currie, Deep-bed filtration under multiple particle-capture mechanisms, Society of Petroleum Engineers Journal 14 (2009) 477–487.
[8] A. Zamani, B. Maini, Flow of dispersed particles through porous media – deep bed filtration, Journal of Petroleum Science and Engineering 69 (2009) 71–88.
[9] A.C. Alvarez, G. Hime, D. Marchesin, P. Bedrikovetsky, The inverse problem of determining the filtration function and permeability reduction in flow of water with particles in porous media, Transport in Porous Media 70 (2007) 43–62.
[10] S. Vigneswaran, R. Ben Aim, Water, Wastewater and Sludge Filtration, CRC Press, Boca Raton, FL, USA, 1989.
[11] K.J. Ives, Theory of filtration. Special Lecture No.7, in: Proceedings of the International Water Supply Association, Eight Congress, Vienna, 1969, vol. 1, pp. K3–K28.
[12] J.P. Herzig, D.M. Leclerk, P. Le Goff, Flow of suspensions through porous media – application to deep filtration, Industrial Engineering Chemistry 62 (5) (1970) 8–35.
[13] C.R. O'Melia, W. Ali, The role of retained particles in deep bed filtration, Progress in Water Technology 10 (5/6) (1978) 167–182.
[14] C. Tien, R.M. Turian, H. Pendse, Simulation of the dynamic behavior of deep bed filters, Journal of American Institute of Chemical Engineers 25 (3) (1979) 385–395.
[15] A. Adin, M. Rebhun, A model to predict concentration and head-loss profiles in filtration, Journal of American Water Works Association 69 (8) (1977) 444–453.
[16] J.C. Crittenden (Ed.), Water Treatment: Principles and Design, 2nd ed., Wiley, 2005.
[17] K.J. Ives, Capture Mechanisms in Filtration in the Scientific Basis of Filtration. Part II, NATO Advanced Study Institute, Cambridge, England, 1973 (Chapter 9).
[18] A. Adin, M. Rebhun, Deep-bed filtration: accumulation-detachment model parameters, Chemical Engineering Science 42 (5) (1987) 1213–1219.
[19] V. Gitis, A. Adin, I. Rubinstein, Kinetic models in rapid filtration, in: Procedures of American Water Works Association Annual Conference, Chicago, IL, 1999.
[20] A.C. Payatakes, C. Tien, Particle deposition in fibrous media with dendrite-like pattern: a preliminary model, Journal of Aerosol Sciences 7 (1976) 85–100.
[21] G. Ziskind, Particle resuspension from surfaces: revisited and re-evaluated, Reviews in Chemical Engineering 22 (2006) 1–123.
[22] J.R. Baylis, Experiences in filtration, Journal of American Water Works Association 29 (12) (1937) 1010–1048.
[23] E.R. Baumann, K.J. Ives, The evidence for wormholes in deep bed filters, in: Proceedings of the Filtech Conference, Utrecht, vol. 1, 1982, pp. 151–164.
[24] K.M. Yao, M.T. Habibian, C.R. O'Melia, Water and wastewater filtration: concepts and applications, Environmental Science and Technology 5 (11) (1971) 1105–1112.
[25] P.V. Danckwerts, Continuous flow systems. Distribution of residence times, Chemical Engineering Science 2 (1) (1953) 1–13.
[26] I. Rubinstein, L. Rubinstein, Partial Differential Equations in Classical Mathematical Physics, Cambridge University Press, Canada, 1993.

[27] C.H. Edwards, D.E. Penney, Differential Equations: Computing and Modeling, 2nd ed., Prentice-Hall College Div, Inc. Pearson Education, Upper Saddle River, NJ, USA, 1999.
[28] S.C. Chapra, Surface Water-Quality Modeling, McGraw-Hill, New York, 1997.
[29] J.F. Atkinson, S.K. Gupta, J.V. DePinto, R.R. Rumer, Linking hydrodynamic and water quality models with different scales, Journal of Environmental Engineering – ASCE 124 (5) (1998) 399–408.
[30] J. Bear, A. Verruijt, Modeling Groundwater Flow and Pollution, Kluwer Academic Publishers, Dordrecht, Holland, 1987.
[31] S. Vigneswaran, K.R. Tulachan, Mathematical modeling of transient behavior of deep bed filtration, Water Research 22 (9) (1988) 1093–1100.
[32] C.U. Choo, C. Tien, Simulation of hydrosol deposition in granular media, AICHE Journal 41 (1995) 1426–1442.
[33] R. Rajagopalan, C. Tien, Trajectory analysis of deep-bed filtration with the sphere-in-cell porous media model, AIChE Journal 2 (1976) 523–533.
[34] R. Rajagopalan, R.Q. Chu, Dynamics of adsorption of colloidal particles in packed-beds, Journal of Colloid and Interface Science 86 (2) (1982) 299–317.
[35] S. Hatukai, E. Gavron, Filtration pilot plant for Israelis national water carrier, International Water & Irrigation Review 16 (3) (1996) 14–19.
[36] V. Gitis, Removal of oocysts of Cryptosporidium parvum by rapid sand filtration. Annual Project Report, IT Corporation for U.S. EPA, Contract No. 68-C-99-211, 2001, 104 pp.
[37] V. Gitis, Rapid sand filtration of Cryptosporidium parvum: effects of media depth and coagulation, Water Science & Technology – Water Supply 8 (2) (2008) 129–134.
[38] T.R. Camp, Theory of water filtration, in: Proceedings of the American Society of Civil Engineers, vol. 90, 1964 (SA4) paper 3990.
[39] S. Vigneswaran, J.S. Chang, Experimental testing of mathematical models describing the entire cycle of filtration, Water Research 23 (11) (1989) 1413–1421.
[40] S. Osmak, A. Glasnovic, The study of filter coefficient behavior using attachment – detachment model for deep bed filtration, Chemistry and Biochemistry Engineering Quarter 8 (4) (1994) 177–181.
[41] A.K. Deb, Theory of sand filtration, Journal of the Sanitary Engineering Division, Proceedings of the American Society of Civil Engineers 95 (1969) 399–422.
[42] Yu.M. Shechtman, Filtration of Low-Concentration Suspensions, Izdatel'stvo AN SSSR, Moscow, 1961 (in Russian).
[43] R.I. Mackie, R.M.W. Horner, R.J. Jarvis, Dynamic modeling of deep-bed filtration, Journal of American Institute of Chemical Engineers 33 (11) (1987) 1761–1775.
[44] C.S.P. Ojha, N.J.D. Graham, Theoretical estimates of bulk specific deposit in deep bed filters, Water Research 27 (1993) 377–387.
[45] Yu.V. Gontar, A modified model of water clarification in filtration through porous media, Khimiya i Tekhnologiya Vody 9 (1987) 487–490 (in Russian).